N93-11964

AN 8-D.O.F. DUAL-ARM SYSTEM FOR ADVANCED TELEOPERATION PERFORMANCE EXPERIMENTS

Antal K. Bejczy and Zoltan F. Szakaly
Jet Propulsion Laboratory
California Institute of Technology
Pasadena, CA   91109

ABSTRACT

This paper describes the electro-mechanical and control features of an 8-D.O.F. manipulator manufactured by AAI Corporation and installed at the Jet Propulsion Laboratory (JPL) in a dual-arm setting. The 8-D.O.F. arm incorporates a variety of features not found in other laboratory or industrial manipulators. Some of the unique features are: 8-D.O.F. revolute configuration with no lateral offsets at joint axes; 1 to 5 payload to weight ratio with 20 kg (44 lb) payload at a 1.75 m (68.5 inches) reach; joint position measurement with dual relative encoders and potentiometer; infinite roll of joint 8 with electrical and fiber optic slip rings; internal fiber optic link for "smart" end effectors; four-axis wrist; graphite epoxy links; high link and joint stiffness; use of an upgraded JPL Universal Motor Controller (UMC) capable of driving up to 16 joints. The 8-D.O.F. arm is equipped with a "smart" end effector which incorporates a 6-D.O.F. force-moment sensor at the end effector base and grasp force sensors at the base of the parallel jaws. The 8-D.O.F. arm is interfaced to a 6-D.O.F. force-reflecting hand controller. The same system is duplicated for and installed at the Langley Research Center.

INTRODUCTION

Most commercially available manipulators have been designed and built with a specific application and performance domain in mind. When it comes to application research and development of a more general nature which typically requires some extra motion dexterity combined with some extra reach and load handling capability together with high positioning accuracy and repeatability, most existing manipulators have shortcomings and have to be modified or rebuilt.

The purpose of the research and development work described in this paper is to build an end-to-end manipulator system to enable the performance of a broad range of realistic tasks not achievable by other manipulators. Of particular interest are tasks like the real-life simulation of the Solar Max Satellite Repair (SMSR) in teleoperation mode. As known, this satellite was not built for maintenance, and was still repaired in Earth orbit in the Space Shuttle bay by two EVA astronauts in 1984. The question now is: can the SMSR task be performed remotely by the use of an advanced telemanipulator system? If so, then what kind of performance can be expected for an SMSR-type work in teleoperation mode?

The SMSR type teleoperation work also raises a number of interesting and important issues regarding redundancy in the kinematics, sensing and control of manipulators and regarding the human operator interface to a redundant manipulator system.

The two 8-D.O.F. manipulators built by AAI Corporation for JPL in 1990 (and two more for LaRC in 1991) serve the purpose of enabling the experimental evaluation of application oriented performance issues briefly indicated above.

In the first part of the paper we summarize the mechanical features of the AAI 8-D.O.F.

arm. The control electronics, including some computational aspects, are briefly outlined in the second part of the paper.

AAI ARM MECHANISM

The Advanced Research Manipulator II (ARM II), Model 1520-8A, is an 8-D.O.F., redundant manipulator designed and built by AAI Corporation (Hunt Valley, MD) to support laboratory telerobotics R & D work. It has a 20 kg (44 lb) payload capacity at a full extension. A high payload to weight ratio is achieved through the use of lightweight graphite epoxy composite materials for the arm links, lightweight modular joints, and high torque servo motors. The ARM II is based on a modular joint design, which permits construction of a wide variety of revolute kinematic configurations. The modular joints are sized according to torque requirements and can be mated to links, regardless of twist angles.

The special kinematic feature of the 8-D.O.F. ARM II is the four-axis, gimballed wrist which allows singularity avoidance in a very wide configuration range and permits small angular changes of the end effector with little or no motion of the lower arm joints. Another special feature of the design is the infinite roll capability of the last, 8th joint to which the end effector is mounted. This permits contiuous rotation about the roll axis of a tool held by the end effector without requiring motion of the other joints.

The ARM II is driven by DC brush motors with integral brakes and encoders. Harmonic drives are used as gear reducers. Each joint is equipped with two encoders for input and output position sensing in the harmonic drives. The encoders are relative position encoders. In addition, each joint is equipped with a potentiometer for sensing absolute position at start up. Each joint also has a thermal sensor, electronic limit switch (except the 8th joint) and a mechanical stop (again, except the 8th joint) outside the limit switch. Some of the motor, brake and gear characteristics are listed in Table 1. Figure 1 shows ARM II, Model 1520-8A as installed at JPL for system integration. Figure 2 shows the cabling system of the arm.

High joint stiffness is achived by the use of high stiffness ball bearings and specially stiffened harmonic drives. Together the two bearings, which have been used in previous space applications, protect the joint against thrust and radial loading. Links 3 and 6 incorporate tubular graphite epoxy elements which provide high stiffness, strength, low weight and structural damping. This last point was experimentally verified on a General Electric P50 robot arm and described in Ref. 2.

The ARM II joint reference frames, following the Denavit-Hastenberg (D-H) convention, together with the D-H parameters are listed in Figure 3. As seen, there are no lateral offsets of joint axes (the a_i D-H parameters are zero for all links). This greatly facilitates the handling of forward and inverse kinematics and dynamic computations. The total reach capability of ARM II is 68.5 inches with the JPL Model C Smart Hand. (Without end effector the reach capability is 60 inches).

Another important feature of ARM II is that stiffness and conservative design constraints allow it to be oriented as desired with respect to gravity. Nonetheless, ARM II is a lightweight manipulator when considering its 1:5 payload to weight ratio. Note that the PUMA 560 payload to weight ratio is 1:13. More on the ARM II design characteristics can be found in Ref. 1.

The mass and inertial characteristics of ARM II links are listed in Table 2. Table 3 lists the ARM II joint natural frequencies. These frequencies are based on motor and harmonic drive inertias without link load inertias since the gear ratios for each joint are sufficiently large to essentially eliminate the load inertia at the motor. Table 3 includes two natural frequencies for two joint stiffnesses: one valid for the very low torque range, K_a, and the other, K_b, valid over the remainder. The lowest natural frequency of the full system is calculated 5.3 Hz and is based on the vibration of joints 2 and 4 under conditions of full load at full extension and assuming that K spring constant applies. The system natural frequency with no payload and full extension
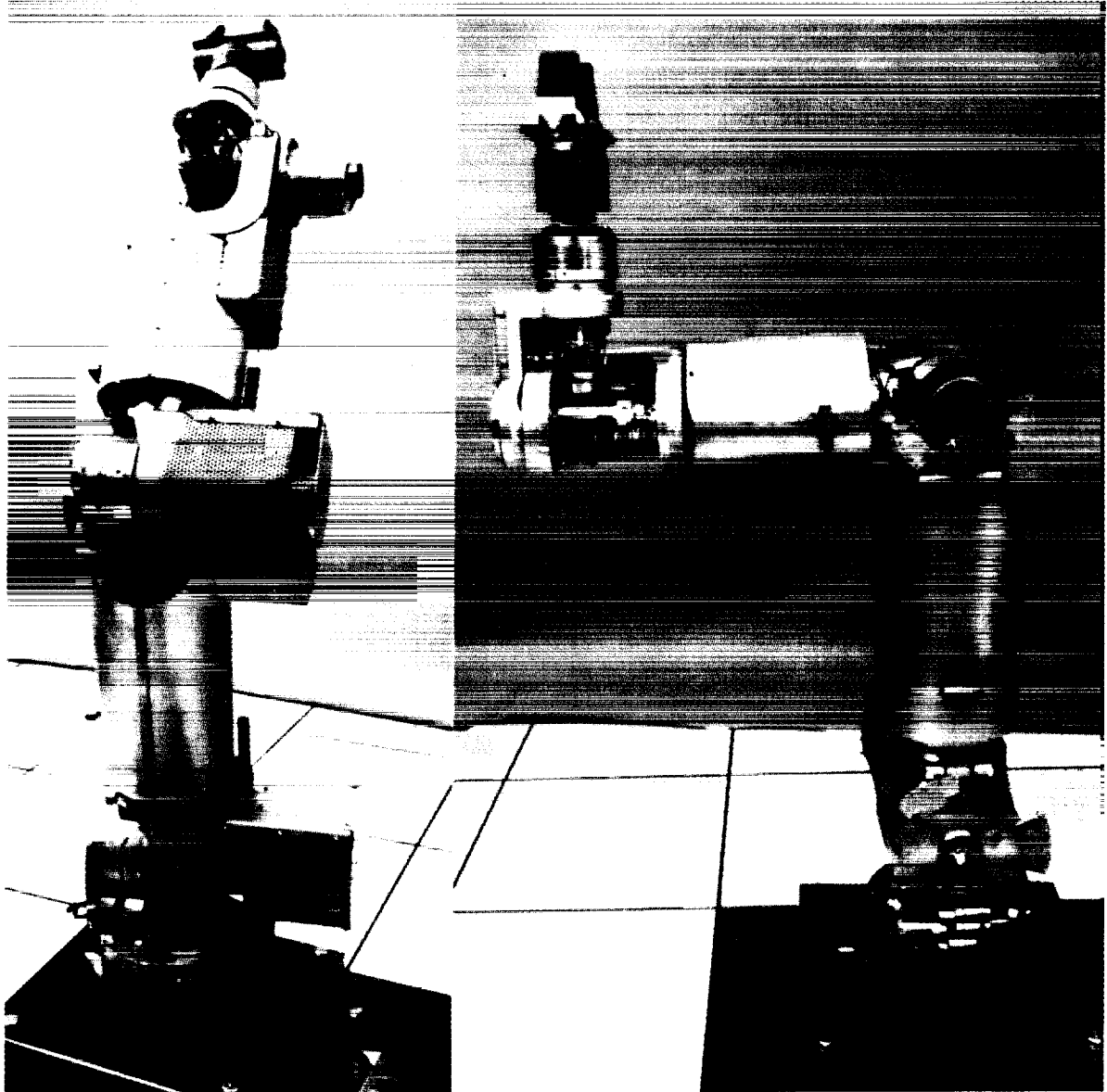
Figure 1. Eight D.O.F. ARM II (by AAI Corporation)

is calculated for 8.4 Hz. This compares well with the lowest natural frequency of the CM T3-776 robot arm measured by Tesar and Behi. This indicates the ARM II is similar to rigid, industrial robot arms in this regard.

The ARM II positional accuracy and repeatability under full load and at full extension is less than $\pm$ 0.1 inches and $\pm$ 0.01 inches, respectively. This is verified experimentally.

The measured maximum tip speed of ARM II

at 30 VDC using only joint 1 motor at full extension was somewhat more than 18 inches per second.

In summary, ARM II incorporates a variety of features not found in other laboratory or industrial manipulators. Some of the unique features are:

- 8 D.O.F. revolute configuration
- Four-axis wrist
- No lateral offsets of joint axes
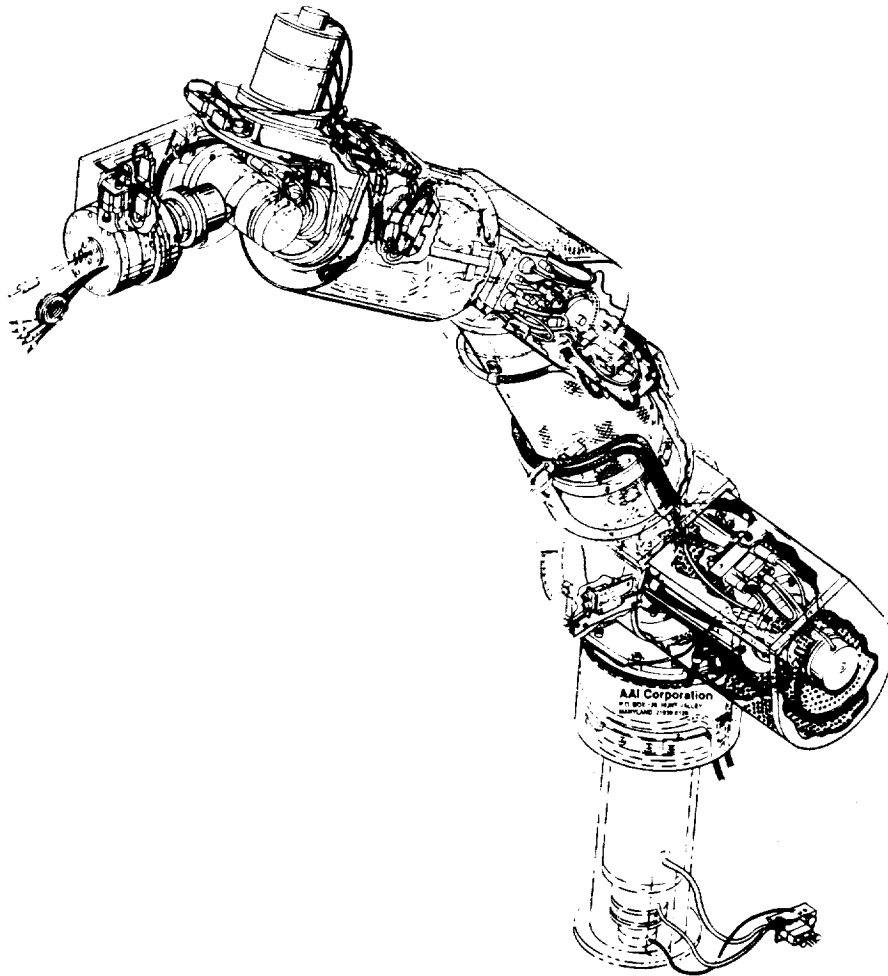- High, 1:5 payload to weight ratio

Figure 2. Eight D.O.F. ARM II Cabling Schematics

- 20 kg (44 lb) payload at maximum extension of arm (60 inches, without end effector)
- Modular joint design
- Graphite epoxy links
- High joint and link stiffness
- Infinite roll of joint 8 with electrical and fiber optic slip rings
- Internal fiber optic link for smart end effectors
- Two techniques for measuring joint position: dual relative encoders and potentiometer
- Indirect measurement of joint torque from dual relative encoders

CONTROL ELECTRONICS

The arms are controlled by a 16 axis UMC (Universal Motion Controller) each. The UMC was designed in our laboratory and it has been commercialized. The commercially available version is sold in four joint increments up to a 16 joint maximum per UMC. We use the commercial UMC ourselves for our various motor controller needs. The AAI arm has eight motors. Each joint, except the last one, is equipped with two optical encoders. There are a total of 15 encoders. These encoders count 4096 for every revolution of the motor shaft. The two encoders are connected to opposing ends of the harmonic drive. The gear reduction is 200 in every joint, so one encoder counts 0.5% slower than the other. Since both encoders are equipped with an index pulse, the two index pulses shift about 2 degrees relative to each other for every motor revolution. (Their relative position can eventually be used to determine absolute joint angle.) Since every joint also has a
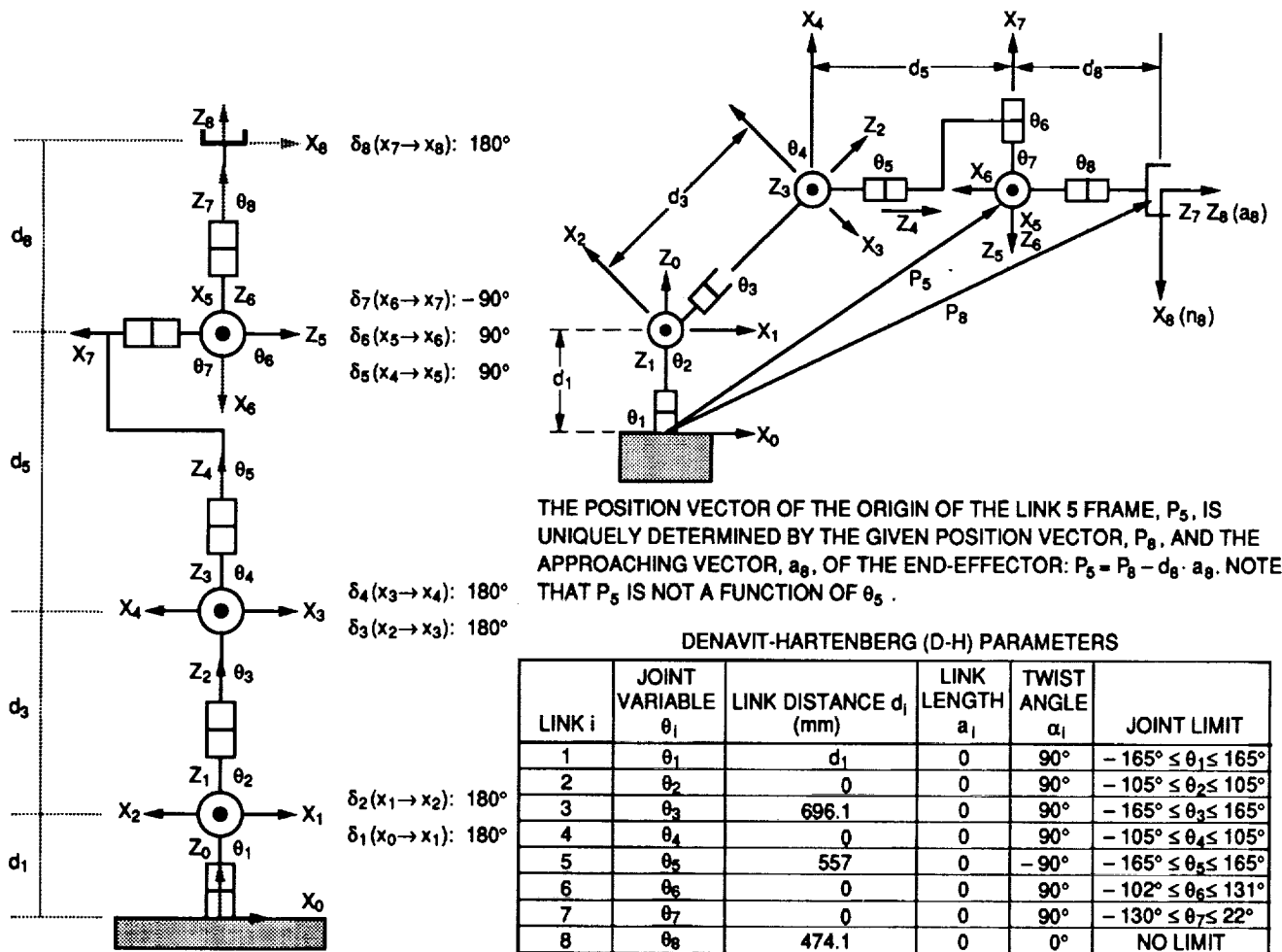
285

Z_8 X_8 $\delta_8 (x_7 \to x_8)$: 180°

Z_7 θ_8

X_5 Z_6 $\delta_7 (x_6 \to x_7)$: −90°

X_7 Z_5 $\delta_6 (x_5 \to x_6)$: 90°

θ_7 θ_6 $\delta_5 (x_4 \to x_5)$: 90°

X_6

Z_4 θ_5

Z_3 θ_4

X_4 X_3 $\delta_4 (x_3 \to x_4)$: 180°

$\delta_3 (x_2 \to x_3)$: 180°

Z_2 θ_3

Z_1 θ_2

X_2 X_1 $\delta_2 (x_1 \to x_2)$: 180°

Z_0 θ_1 $\delta_1 (x_0 \to x_1)$: 180°

X_0

THE POSITION VECTOR OF THE ORIGIN OF THE LINK 5 FRAME, P_5, IS UNIQUELY DETERMINED BY THE GIVEN POSITION VECTOR, P_8, AND THE APPROACHING VECTOR, a_8, OF THE END-EFFECTOR: $P_5 = P_8 - d_8 \cdot a_8$. NOTE THAT P_5 IS NOT A FUNCTION OF θ_5.

DENAVIT-HARTENBERG (D-H) PARAMETERS

LINK i	JOINT VARIABLE θ_i	LINK DISTANCE d_i (mm)	LINK LENGTH a_i	TWIST ANGLE α_i	JOINT LIMIT
1	θ_1	d_1	0	90°	$-165° \le \theta_1 \le 165°$
2	θ_2	0	0	90°	$-105° \le \theta_2 \le 105°$
3	θ_3	696.1	0	90°	$-165° \le \theta_3 \le 165°$
4	θ_4	0	0	90°	$-105° \le \theta_4 \le 105°$
5	θ_5	557	0	−90°	$-165° \le \theta_5 \le 165°$
6	θ_6	0	0	90°	$-102° \le \theta_6 \le 131°$
7	θ_7	0	0	90°	$-130° \le \theta_7 \le 22°$
8	θ_8	474.1	0	0°	NO LIMIT

Figure 3. Zero Configuration of the Eight D.O.F. ARM II. The Joint Offset, δ_i, i = 1, ... , 8, are Defined as the D-H Angles at the Zero Configuration.

potentiometer, there are two ways to determine the absolute position of the arm. The two encoders provide two sources to determine the relative position. This is the primary quantity used for control. The load on the joint causes windup in the harmonic drive mechanism, this windup is precisely detected by the shift of one encoder position relative to the other. This is a way to determine joint torque. The alternative way is to read the motor current from the UMC.

The UMC is a cage housing two major subsystems, the multiprocessor and the motor control and sensing subsystems. (See Figure 4). Currently the multiprocessor subsystem consists of up to 8 processors. These are NS 32016 boards interconnected by a MULTIBUS -I backplane. These processors perform about 1 MIPS. All of our

computations are currently done in this environment. We are developing a new high performance multiprocessor system that will be based on a custom designed high speed bus and processors in the 10 to 15 MIPS range each. We will describe that in more detail subsequently. The other major subsystem of the UMC is the motor controller. The motor controller consists of the following:

Joint processor
Joint interface
Power amplifiers
Input filters

The joint processor is one 32016 board dedicated to controlling the joints. It interfaces to the joint interface cards via a 16 bit i/o bus. This i/o bus is built to the

286

Table 1. Some Drive System Features of ARM II

Joint	MOTOR				Brake Rated Torque (oz-in)	Gear Ratio
	Rated Speed (rpm)	Rated Torque (oz-in)	Rated Current (A)	Rated Volt (V)		
1	1970	861	12.9	120	1200	200
2	1970	861	12.9	120	1200	200
3	2164	285	10.5	60	560	200
4	2164	285	10.5	60	560	200
5	1600	162	7.25	40	240	200
6	3000	86	7.8	35	128	200
7	1600	162	7.25	40	240	200
8	2050	51	4.9	30	240	200

Table 2. Mass/Inertia Parameters for Dynamic Model of AAI ARM II, Given in the Individual Link Reference Frames

Link & Reference Frame i	Mass (lb.s²/in) M_i	Mass Center (in)			Moments of Inertia (in.lb.s²)			Reflected Rotor Inertia I_{a_i} ** (in.lb.s²)
		M_{X_i}	M_{Y_i}	M_{Z_i}	I_{XX_i}	I_{YY_i}	I_{ZZ_i}	
0	X	X	X	X	X	X	X	356
1	.1612	0.0	3.50	-4.05	12.34	5.882	7.334	356
2	.0764	0.0	.83	18.15	29.09	28.96	.4023	80.7
3	.0682	0.0	2.43	-2.06	2.499	1.378	1.528	80.7
4	.0682	3.22	0.0	15.62	18.81	20.45	1.904	52.1
5	.0455	-.37	0.0	-.90	.2199	.3419	.2044	16.3
6	.0336	-3.53	-.04	1.60	.2699	.9204	.7414	52.1
7 *	.0077	0.0	0.0	9.5	.7090	.7090	.0195	27.1

*) Without End Effector Data
**) Includes ALL Input Shaft Inertias Multiplied by the Square of the Gear
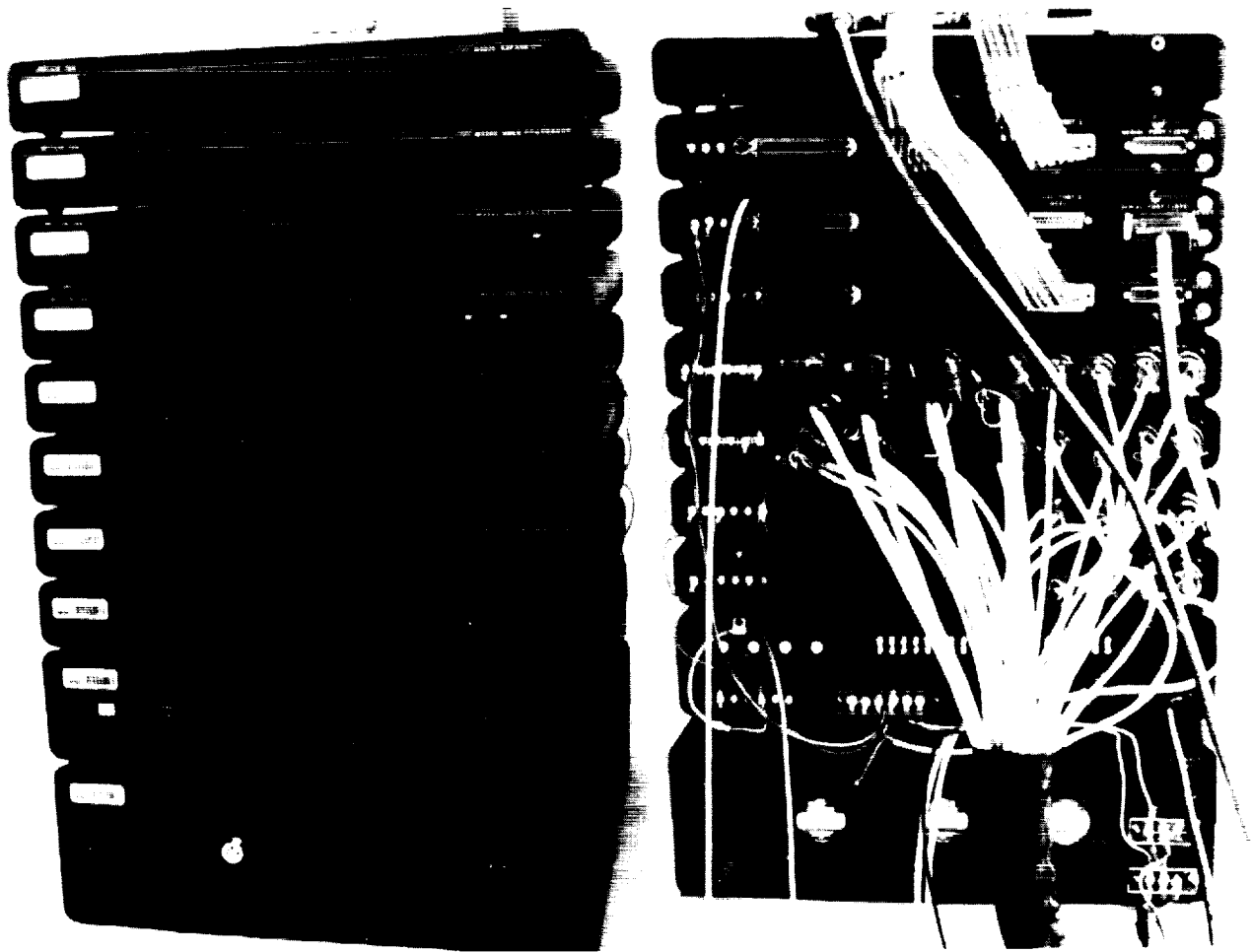Ration Between Input/Output

Figure 4. Eight D.O.F. ARM II Control Electronics, in Front and Rear Views

Table 3. Joint Natural Frequencies

Joint	Natural Freq. (Hz)		Spring Constant (10^5 lb in/rad)	
	w_a	w_b	A	B
1	6.9	10.0	9.0	18.8
2	6.9	10.0	9.0	18.8
3	6.9	9.9	2.5	5.15
4	6.9	9.9	2.5	5.15
5	8.7	12.7	1.1	2.34
6	11.1	27.1	0.48	1.20
7	8.7	12.7	1.1	2.34
8	27.1	39.5	1.1	2.34

Intel iSBX standard. The i/o bus makes the joint motion parameters memory mapped to the joint processor's address space. The joint interface card performs input data conversion and output control functions to the power amplifiers.

Each joint interface card has the following functions:

- 16 analog input channel A/D converter at a 12 bit accuracy.
- 4 optical encoder position counters.
- 4 digital tachometers.
- 4 digital control units for the PWM amplifiers.
- EEPROM non-volatile memory to store joint parameters.
- Watchdog timer.

288

The optical encoder interface is an up/down counter that can be used in 8 or 12 bit modes. The count has to be read periodically by the software to avoid more than one wraparound. *The software computes the incremental change from one reading to the next and adds this change to a counter in memory.

The digital tachometers are devices that measure the time lapse from one positive edge in the input encoder pulse stream to the next. The software divides a constant with this time to get a quantity that is proportional to the joint velocity.

The PWM amplifiers in the UMC are controlled by digital signals that are generated on the joint interface cards. Each joint has two controlling registers, the motor is driven at a duty cycle that corresponds to the smaller value of the two. This arrangement ensures software control of the motor voltage even in case of component failures in the system. The amplifiers used to drive the AAI arm can deliver 20A of current at 60V each.

The PWM amplifiers in the UMC are unique in the sense that they do not have an integral current feedback loop. Conventional PWM circuits are strongly non linear. This necessitated the use of a feedback loop that linearizes the current transfer function of the amplifier. Such PWM amplifiers take an analog signal as input and produce a motor current on the output. The amplifiers in the UMC are designed such that the relationship between duty cycle and motor voltage, current and energy output is linear. This makes it unnecessary to have a feedback loop inside the amplifier. The output can be controlled directly with a digital signal, eliminating an intermediate analog stage. It is also because of this that the amplifiers produce an inherent velocity damping due to the tachometer effect of the motor. This reduces the magnitude of additional velocity damping needed. In such a system the motor itself is used as a tachogenerator, without any additional hardware. More on the UMC can be found in Refs. 4 and 5.

Input filters are also implemented since they are needed because the sharp rising and falling edges of the PWM signals driving the

motor generate high energy noise spikes on all of the incoming signals. Such spikes are relatively easy to filter out because they are narrow. The incoming digital signals are first filtered by an R-C low-pass filter, after which a four stage digital sampling filter eliminates all pulses that are narrower than 2 microseconds. The analog signals are R-C filtered once in the input filter section and a second time on the joint interface card.

Control Computations

The multiprocessor system presently contains a total of three processors. The computer hardware system, including communication to the control station computer mode (and to the VME bus at the LaRC installation) are shown in Figure 5. The computational functions are distributed among the three processors as follows:

- Remote communication, trajectory generation, Cartesian servo and harmonic motion generator.
- Inverse and forward kinematics, gravity compensation, smart hand interface and compliance.
- Joint servo

The remote communication consists of a packet exchange via the fiber optic link. The hand controller node transmits a packet to the robot node. This packet contains a mode byte, a six byte (one for each degree of freedom) relative motion command, a one byte grasping force command and a checksum. When the robot node receives this packet it replies with its own that contains the following: Currently active control mode, robot position in the task space and joint space, the forces on the end effector, the finger position and a checksum.

The trajectory generator receives the incremental motion commands from the communication and generates the desired joint or task space positions for the robot. In one of the joint modes this is simply an addition of the incoming command to the joint setpoint. In task mode the input matrix for the inverse kinematics has to be generated. This consists of the end effector tip position which is generated by simple accumulation and the end effector

FRHC: FORCE-REFLECTING HAND CONTROLLER
FO: FIBER OPTIC
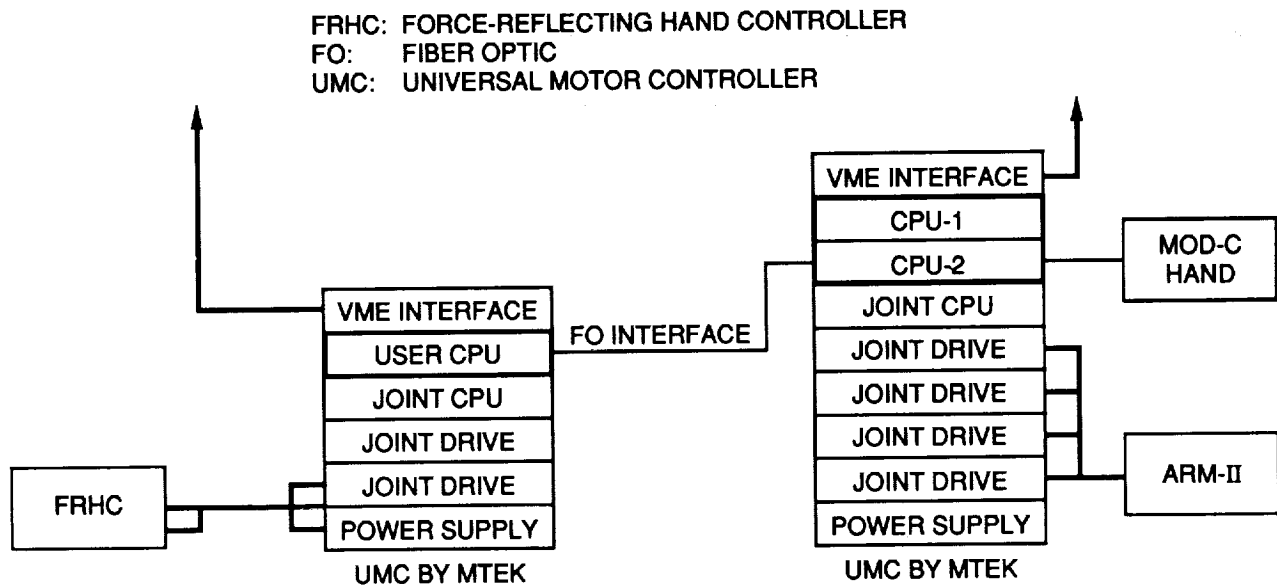UMC: UNIVERSAL MOTOR CONTROLLER

Figure 5. Eight D.O.F. ARM II Overall Control Schematics (Also Indicating VME Bus Interface at LaRC)

orientation matrix which is computed by consecutive rotations of this matrix while maintaining its orthonormality. When switching from one mode to another continuity of the robot position is maintained. This is accomplished by feeding the output of the forward kinematics into the input of the inverse kinematics while not in task mode.

The Cartesian servo improves trajectory tracking accuracy by establishing a servo loop in the task space. This servo loop compares the output of the forward kinematics to the desired Cartesian position and applies a correction to the input of the inverse kinematics to reduce the error.

The harmonic motion generator allows the robot to execute autonomous motions. These motions currently consist of straight line segments but curved segments will later be introduced. The tip velocity of the robot is controlled as a function of the position along the line of motion. This velocity has a sinusoidal profile. The compliance parameters can be independently preset for every motion segment. This allows the robot, for example, to autonomously track the inside edge of a hole or the outside envelop of an object. More on Cartesian Servo and Harmonic Motion Generator can be found in Refs. 6 and 7.

The inverse and forward kinematic computations are solved as an integrated package. The mathematics are based on the work performed in our group at JPL. (See Ref. 3). The governing principle in the computations is to use geometric reasoning to achieve optimum performance. One joint of the first four and one joint of the last four are parametrized, they maintain their positions from the last time they were moved in joint mode. The remaining six joints are computed based on the tip position and orientation requirement.

The gravity compensation precomputes the torque load of each joint based on the static weight of the links. This value is added to the feed forward field of the UMC joint servo. Such compensation improves the robot positioning accuracy substantially.

The smart hand interface controls the trimming values of the input channels of the smart hand force sensor, it controls the grasping and it reads the wrist force torque information. The forces and torques are converted to the laboratory frame and they are also low pass filtered. From the basic 500 Hz force readings a 100 and a 5 Hz force is generated. More on the Smart Hand can be found in Ref. 8.

290

The compliance function modifies the desired Cartesian position according to the forces detected. There are two types of compliance, spring and rate type. The spring type of compliance causes the robot position to be proportional to the force acting on it. This is equivalent to a spring. The integrating compliance causes that the velocity is proportional to the force on the tip. This is equivalent to a viscous damping. The two types of compliances can be mixed with each other as desired. More on compliance control can be found in Refs. 5 and 6.

The joint servo function is performed by a dedicated processor. This processor runs the code generator software. The code generator has a set of menues on which the user defines the robot being controlled. Based on this information the code generator writes highly optimal machine code that controls the robot. This makes it possible to switch polarities of various devices at runtime without changing the hardware, to move a joint from one output port to the next to facilitate debugging and to safely setup a new robot without risking damage to the hardware. This software also performs calibration at power on time to establish the robot absolute position accurately. Currently we cannot utilize the multiple redundancies of the robot fully because special software will have to be written that recognizes the failure of various devices and switches over to their alternative.

The control modes are the following:

- Freeze mode
- Neutral mode
- Joint - 1
- Joint - 2
- Task

Freeze mode means that the robot does not move and the brakes are all set. This is an alternative to the robot being completely turned off.

Neutral mode allows the robot to be moved by hand, it is gravity compensated but the control gains are set to 0.

The two joint modes allow the operator to control the joints using the hand controller. In joint-1 the upper and lower arm rotations are controlled, in join-2 the remaining six joints move.

Task mode controls the end effector position and orientation via the inverse kinematics. The current implementation freezes the joint 3 and 5 positions.

Advanced Bus, Advanced Processor

Due to the limited processing performance of our current system (1 MIPS per processor) and the limited transfer rate of our bus (MULTIBUS-I) we coded all of our computations in 32000 assembly language. The arithmetic is performed using binary fixed point instructions to gain execution time. Currently the control systems for the two (right and left) robots are not tightly coupled to each other. It is desirable for us to control both robots from the same tightly coupled environment and to increase our processing and bus communication performance. The only viable commercial alternative at hand would be a VME bus system. It is generally agreed upon by the research community today that the VME bus is no longer fast enough to support a high number of high performance processors working in a closely coupled environment. In fact, it is our view that the very concept of the bus for our application has to be rethought instead of just trying to build yet another bus that is a little faster then the previous ones.

For these reasons we came up with an advanced bus concept to support our new high performance multiprocessor environment. This system will have up to 16 processors on a bus with 10 or 15 MIPS of performance each. This new bus concept delivers about 10 times the performance of a VME bus at the same clock rate, and will be clocked at 20 MHz so we expect a better than 20 fold performance increase relative to VME bus systems. The processors will use fiber optic links as their primary means of communication outside the cardcage. Each of our processors will have 4 Mbytes of dynamic memory as well as a floating point processor and various i/o functions.

This new bus architecture brings several improvements in addition to the increased data processing capabilities. Since the arbitration on the bus is completely eliminated, the processors do not handshake to each other when the information is transferred. This makes it possible for several people to develop their software at separate locations and perhaps even using different programming languages. Once the programs are debugged they can be downloaded into the multiprocessor system and used. A number of processors can be running their software simultaneously while one of them is stopped and a new version of the software is downloaded and started. The program execution times do not change when a software piece is transferred from a single processor to the multiprocessor environment.

In a conventional bus system the bus load is not uniform. For example, if there is a common servo period there will be more traffic on the bus at the beginning and the end than in the middle in between. In a traditional bus every processor has to acquire control of the bus signals through arbitration before it can transfer data. This transfer could be either reading and writing. Typically a data item that is of global interest is generated once in a servo period and it is read several times by various different processors.

In our advanced bus the data is written into a FIFO register the time it is generated. The processor where the data is broadcast to all processors that need it simultaneously. Subsequently every processor will read its own copy as many times as needed without going to the bus. Since the transactions wait in their FIFOs till the bus can take them, bus overload cannot happen during peak traffic periods. The bus will only saturate if the long time average of the traffic exceeds the bus transfer capacity of 80 Mbytes/seconds. In comparison a VME bus will experience difficulties as soon as the momentary traffic exceeds about 4 Mb/s. The true bandwidth of a VME bus can only be utilized well if there is a single processor controlling the bus for an extended period of time.

The planned advanced bus and advanced processor will greatly facilitate the real-time (or, near-real-time) implementation of algorithms which are implied in the methodology that we have adopted for handling redundancy of the 8-D.O.F. AAI arms.

Methodology for Redundancy Handling

The proposed method for the inverse position transformation is based on parameterizing selected redundant joints in order to reduce the problem to a deterministic level. The solution is now based on the previously assigned, but adjustable values of parameters. For a class of robots for which arm decomposition is possible, arm redundancy can be distributed to individual subarms, such that a closed form of parameterized inverse kinematic solutions can be readily obtained from the subarm kinematics. The Null Space Manifold is then formed in the parameter space and characterized with an artificial potential field to represent manipulator internal as well as external behavior. The null space manifold can be easily scanned by varying the parameter values within their limits, and by checking the availability of the solution in the deterministic level. The artificial potential field over the null space manifold is formed based on a combination of several desired attributes such as the proximity to joint limits, the proximity to singularities, the proximity to current configuration, and the measure of static and dynamic manipulabilities.

The artificial potential field over the null space manifold can be used for the optimal adjustment of parameter values either automatically or manually by an operator. The automatic adjustment of parameter values is based on the local gradient of the potential field. Alternatively, a globally optimal joint trajectory can be formulated by analyzing the variation of the potential field at successive task points along the given task trajectory. The parameterization method also allows the visualization of manipulator internal performance through the display of a potential field in the parameter space. This provides a medium

for interactive interface between operator and manipulator for advanced teleoperation, through which the operator can decide whether, when and how to reconfigure the arm for optimal task execution. More on this methodology and related computational algorithms and techniques can be found in Ref. 3.

REFERENCES

1. P. D. Spidaliere, "The Advanced Research Manipulator II: Design and Research Opportunities," to appear in Springer Verlag book "Robots with Redundancy," NATO Advanced Research Workshop, Salo, Italy, July 1988.

2. B. S. Thompson, et al., "An Experimental Investigation of an Articulated Robotic Manipulator with a Graphite Epoxy Composite Arm," Journal of Robotic Systems, Vol. 5, pp. 73-79, 1988.

3. S. Lee and A. K. Bejczy, "Redundant Arm Kinematic Control Based on Parametrization," Proc. 1991 IEEE Int'l Conf. on Robotics and Automation, Sacramento, CA, April 9-11, 1991.

4. A. K. Bejczy and Z. F. Szakaly, "Universal Computer Control System for Space Telerobots," Proc. 1987 IEEE Int'l Conf. on Robotics and Automation, Raligh, NC, March 31-August 3, 1987.

5. Bejczy, A. K., Szakaly, Z., Kim, W. S., "A Laboratory Breadboard System for Dual-Arm Teleoperation," Proc. of Third Annual Workshop on Space Operations, Automation and Robotics, JSC, Houston, TX, July 25-26, 1989, NASA Conf. Publication 3059, pp. 649-660.

6. Szakaly, Z. and Bejczy, A. K., "Performance Capabilities of a JPL Dual-Arm Advanced Teleoperations System," Proc. of SOAR'90 Workshop, Albuquerque, NM, June 26, 1990, pp. 30-41.

7. Bejczy, A. K., Szakaly, Z., "A Harmonic Motion Generator for Telerobotic Applications," Proc. of IEEE Intl. Conf. on Robotics and Automation, Sacramento, CA, April 9-11, 1991, pp. 2032-2039.

8. Bejczy, A. K., Szakaly, Z., Ohm, T., "Impact of End Effector Technology on Telemanipulation Performance," Proc. of Third Annual Workshop on Space Operations, Automation and Robotics, JSC, Houston, TX, July 25-27, 1989, NASA Conf. Publication 3059, pp. 429-440.